Eur. Phys. J. B **14**, 725–732 (2000)

THE EUROPEAN PHYSICAL JOURNAL B

EDP Sciences

Persistent currents in mesoscopic cavities and the effect of level crossings as random variables

A.J. Fendrik and M.J. Sánchez[a]

Departamento de Física J.J. Giambiagi, Facultad de Ciencias Exactas y Naturales, Universidad de Buenos Aires, Ciudad Universitaria, 1428 Buenos Aires, Argentina

Received 5 July 1999

Abstract. In the present article we perform analytical and numerical calculations related to persistent currents in 2D isolated mesoscopic annular cavities threaded by a magnetic flux. The system considered has a high number of open channels and therefore the single particle spectrum exhibits many level crossings as the flux varies. We determine the effect of the distribution of level crossings on the typical persistent current.

PACS. 73.23.Ra Persistent currents

1 Introduction

Recent developments in micrometer-scale technology have made possible the fabrication of devices small enough to make electrons phase-coherent inside. Therefore the transport properties of those samples at very low temperatures exhibit features characteristic of quantum coherence of the electronic wave function along the sample. The observed Aharonov-Bohm oscillations in the resistance of a loop pierced by a magnetic flux is one of the most relevant manifestations of the interference phenomena typical of phase coherence [1,2].

Although the transport properties have been intensively investigated both theoretically and experimentally, the persistent current problem remains less well-understood. In 1983 Büttiker, Imry and Landauer, following earlier work by Byers and Yang on superconducting rings [3], proposed the existence of such currents in one-dimensional mesoscopic loops in the presence of weak magnetic fields [4]. These equilibrium currents are a consequence of the nature of the eigenfunctions and their flux sensitivity, which is strictly of the Aharonov-Bohm type. The current is a periodic function of the magnetic flux with fundamental period $\phi_0 = hc/e$. In ideal clean rings at 0 K (ballistic regime) the current is proportional to $I_0 \equiv ev_{\rm F}/L$ where $v_{\rm F}$ is the Fermi velocity and L is the length of the loop. On the other hand, in the diffusive regime (when impurities are present and the elastic mean free path l is shorter than the typical sample size) theoretical studies predict that the current decreases by a factor l/L. The problem of persistent currents did not deserve much attention until recent years when experimental measurements have been performed on metallic rings in the diffusive regime [5,6] and in a few-channel mesoscopic semiconductor ring [7]. For the metallic systems, the experimental value of the current is $\sim (0.3-2)I_0$, 1 or 2 orders of magnitude greater than the theoretical predictions consistent with diffusive motion, that is with no apparent corrections due to disorder. The value of the current reported by Mailly and collaborators on the mesoscopic ring, is also of the order of I_0, but in their experiment $l/L \sim 1$.

Owing to the discrepancies between the observed and predicted values of the current, many theoretical efforts were made in order to find a mechanism which could compensate the effect of impurities. We are not going to describe these approaches here. For a recent review of the problem, see [9].

Most of the theoretical studies mentioned above where restricted to one-dimensional geometries [10]. The effect of the number of channels in the persistent current, although investigated by many authors, is not yet completely understood. The computations of these currents in 2D (multichannel) geometries is much more difficult, and all the studies for multichannel geometries have been performed employing discrete models or cylindrical geometries in which the transverse channels are decoupled for the conduction mode [11–13].

In this paper we deal with the persistent current problem for a system of N non-interacting electrons confined in a mesoscopic clean annular 2D geometry at 0 K. This geometry is useful to describe the real metallic "rings" employed in most of the experiments mentioned above. As an example in reference [7] the ring has an internal diameter of 2 μm and external diameter 3.4 μm, forming a 2D cavity. The quoted temperature of this experiment (15 mK) and the geometry of the sample make the single particle level mean spacing greater than

[a] e-mail: majo@df.uba.ar

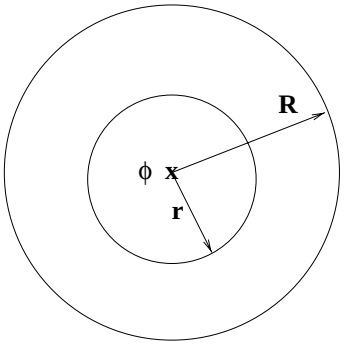

Fig. 1. Annular billiard threaded by a magnetic flux ϕ. The internal and external radii are denoted r and R respectively.

the thermal factor KT. For such a situation we expect that the features of the single particle spectrum become relevant to describing the persistent current problems in a pure quantum regime. The semiclassical limit for these systems was recently reviewed by Richter *et al.* in [8].

Our system is formally a quantum billiard whose Hamiltonian H depends on a parameter (the magnetic flux). The variation of the parameter preserves the commutator $[H, L] = 0$ (L being the angular momentum), and therefore the single particle spectrum displays a large number of crossings as the parameter is varied [14]. Such degeneracies and their features are fundamental ingredients which affect the persistent currents when many channels are open. In fact, they are not only responsible for the multiple jumps that the persistent currents show as a function of flux (for fixed number of particles N) but also for the large oscillations in the typical current as a function of N after averaging on the flux. These oscillations (which are inherent to the system because they depend on the features of the crossings of the single particle energy levels) make it difficult to establish an average behaviour with N. In the present work we show that not only the actual average behaviour but also the large oscillations emerge when the statistical properties of the degeneracies are considered.

The paper is organized a follows. In Section 2, we present our system (we call it the Aharonov-Bohm annular billiard). Section 3 is devoted to summarize some results and properties of persistent currents in 1D and 2D. In Section 4, we introduce the properties of level crossings that allow us to perform a statistical approach to the problem. Section 5 is addressed to exploit the properties of the level crossings in order to determine the dependence of the average behaviour and the fluctuation of the persistent current on the number of particles N. Finally, in Section 6 we present concluding remarks.

2 The Aharonov-Bohm annular billiard

We consider a 2D structure with the geometry of an annulus (see Fig. 1). The cavity consists of a planar region limited by two concentric circles of outer and inner radii R and r respectively. In the following we will take the area equal to π and define the parameter $\lambda = R/r$. The spatial degrees of freedom are the azimuthal angle θ and the radial coordinate ρ which varies between r and R.

Let N be the number of non-interacting electrons in the cavity. We are interested in the persistent current caused by the application of a homogeneous time independent magnetic flux ϕ threading the cavity axially. We disregard the effects of the magnetic field piercing the body of the annulus, so the electrons move with uniform rectilinear motion inside the cavity. We choose the gauge in which $\mathbf{A} = \phi/(2\pi\rho)\ \boldsymbol{\theta}$ where $\boldsymbol{\theta}$ is the azimuthal unit vector.

The single particle spectrum results from the eigenvalue equation

$$\Delta\Psi + \frac{2\mathrm{i}\alpha}{\rho^2}\frac{\partial\Psi}{\partial\theta} - \frac{\alpha^2}{\rho^2}\Psi + k^2\Psi = 0 \qquad (1)$$

where Δ is the Laplacian in polar coordinates. We define the scaled flux $\alpha = \phi/\phi_0$ and we use units such that $\hbar^2/2m = 1$, so the energy is $E = k^2$.

We apply Dirichlet boundary conditions at $\rho = r$ and $\rho = R$, and periodic boundary conditions in the azimuthal direction.

Equation (1) is separable in polar coordinates and we factorize $\Psi(\rho, \theta) = \mathcal{F}(\rho)\exp \mathrm{i}m\theta$ with $m = 0, \pm1, \pm2...$ the orbital quantum number. The eigenfrequencies $k_{\nu,n}$ result from the solution of equation

$$J_\nu(z\lambda)N_\nu(z) - J_\nu(z)N_\nu(z\lambda) = 0, \qquad \nu = m + \alpha, \quad (2)$$

where we have defined $z \equiv kr$ and $n = 1, 2...$, is the radial quantum number. J_ν and N_ν are the Bessel functions of the first and second kind, respectively. The corresponding eigenfunctions $\Psi(\rho, \theta)$ are:

$$\Psi_{\nu,n}(\rho,\theta) = A_{\nu,n}[J_\nu(k_{\nu,n}\rho)N_\nu(k_{\nu,n}r) - J_\nu(k_{\nu,n}r)N_\nu(k_{\nu,n}\rho)]\exp(\mathrm{i}m\theta) \quad (3)$$

where $A_{\nu,n}$ is the normalization constant.

All the eigenstates and all the equilibrium physical properties of the system are periodic functions of the flux with period ϕ_0 [3]. Moreover since the energy spectrum is symmetric with respect to $\phi = \phi_0/2$, in the following the parameter α will take values between 0 and 1/2. For $\alpha \neq 0$, the states with m and $-m$ are, in general, nondegenerate. This is the reason for the existence of an equilibrium persistent current.

We stress that for the present system $E_{\nu,n}$ cannot be written down as a simple function of the numbers ν and n as it happens, for example, in the cylindrical geometries in which the eigenenergies are quadratic functions of the quantum numbers. This constitutes the fundamental difference between the annular cavity and other 2D geometries studied so far, [10].

To obtain the eigenenergies $E_{\nu,n}$ we have numerically solved equation (2). For each fixed value of λ, m and n, we have taken six equally spaced values of α between 0 and 1/2. Then we have verified that the best quadratic fit was

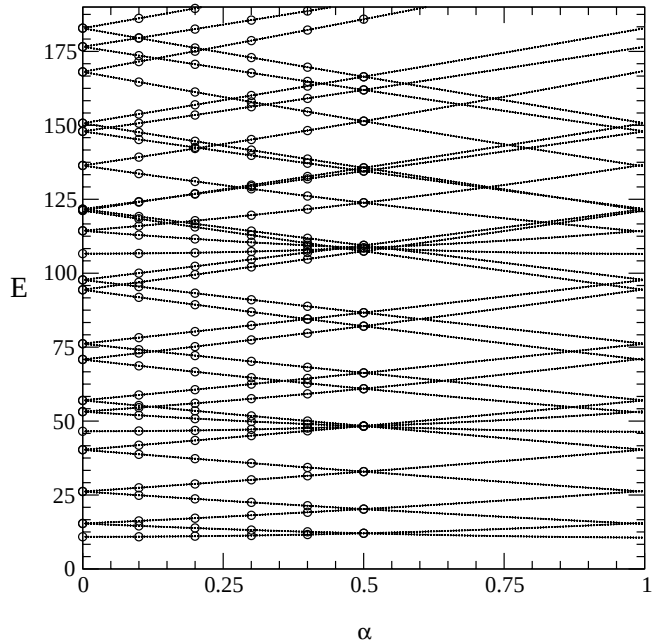

Fig. 2. Single particle energy levels as a function of the adimensional flux α, corresponding to the lowest region of the spectrum for the annular billiard with $\lambda = 10$. The circles correspond to exact values obtained from the zeros of the cross products of Bessel functions. The lines of small dots are the quadratic fits. See the text for details.

quite satisfactory for the considered values of λ. Figure 2 shows a region of the energy spectrum as a function of α for $\lambda = 10$ obtained by the described procedure. In the following we will consider

$$E_{m+\alpha,n} = A_{m,n}(\lambda)\alpha^2 + B_{m,n}(\lambda)\alpha + C_{m,n}(\lambda). \qquad (4)$$

Let us remark that for the cylindrical geometries (*i.e.* a cylindrical surface of area $L \times L_y$) the coefficients can be determined exactly and they are, $A = (2\pi/L)^2$ (without any dependence on the quantum numbers) and $B = 2m(2\pi/L)^2$ which depends only on the orbital quantum number m. The other quantum number appears only in the constant term C.

3 Persistent currents in N electron systems

In the present section we summarize the main results concerning persistent currents in 1D (rings) and 2D (cylinders and annular) systems.

For a system with N non-interacting electrons, the total current is $I_{\rm T} = \sum_{n=1}^{N} I_n$ [10].

In order to characterize the typical current we define $I_{\rm typ} = \sqrt{\langle I_{\rm T}^2 \rangle_\alpha}$, where the symbol $\langle .. \rangle_\alpha$ means flux average. This is

$$I_{\rm typ}^2 = 2\int_0^{1/2} I_{\rm T}^2 \, {\rm d}\alpha; \qquad (5)$$

where we have profited from the symmetry of the spectrum with respect to $\alpha = \frac{1}{2}$.

3.1 1D systems

For a 1D ring of circumference L threaded by a magnetic flux ϕ, the velocity of an electron in the state with orbital quantum number m is $v_m = \frac{1}{\hbar}\partial E_m/\partial k_m$. Therefore as $k_m = 2\pi(m+\alpha)/L$, the current carried by the level E_m results [10]

$$I_m = -\frac{\partial E_m}{\partial \phi} \cdot \qquad (6)$$

It is well-known that for the 1D ring geometries, the crossings between levels in the range $0 \le \alpha \le 0.5$ occur only for $\alpha = 0$ or $\alpha = 0.5$. This fact is a direct consequence of the existence of only one channel in the system. The total current for the N-electron system is,

$$I_{\rm T} = \begin{cases} \dfrac{-2e}{L^2}\pi N\alpha & N \text{ odd} \\ \dfrac{-e}{L^2}\pi N(2\alpha - 1) & N \text{ even,} \end{cases} \qquad (7)$$

where we have explicitly used $k_{\rm F} = \pi N/L$. Therefore the typical current is $I_{\rm typ} \sim N$. This is consistent with the well-known result for 1D geometries, $I_{\rm typ} = I_0$ with $I_0 \equiv ev_{\rm F}/L$ [10].

3.2 2D systems

In the case of 2D cylindric geometries, as the energy of an individual state is separable into two terms, one associated with the conduction mode and the other with the transversal one, it is straightforward to verify equation (6). For the annular geometry, this equation is not obvious. In order to prove equation (6) we begin computing the current density $\mathbf{j}$:

$$\mathbf{j} = \frac{1}{2m}\left[\Psi^*\left(-{\rm i}\hbar\nabla + \frac{e}{c}\mathbf{A}\right)\Psi + \Psi\left({\rm i}\hbar\nabla + \frac{e}{c}\mathbf{A}\right)\Psi^*\right]. \qquad (8)$$

From equation (1) it is straightforward to show that

$$\frac{\partial \mathcal{H}}{\partial \phi} = \frac{e}{mc}\left[-{\rm i}\hbar\nabla + \frac{e}{c}\mathbf{A}\right]\frac{\partial \mathbf{A}}{\partial \phi} \cdot \qquad (9)$$

Comparing equation (9) and equation (8), we obtain

$$\frac{2e}{c}\mathbf{j}\frac{\partial \mathbf{A}}{\partial \phi} = \Psi^*\frac{\partial \mathcal{H}}{\partial \phi}\Psi + \Psi\left(\frac{\partial \mathcal{H}}{\partial \phi}\right)^*\Psi^*.$$

Taking into account the functional form of the vector potential $\mathbf{A}$ and the Hellmann-Feynman theorem [15], the current carried by the state i results:

$$I_i \equiv -e\int j_\theta \, {\rm d}\rho = -c\frac{\partial E_i}{\partial \phi}, \qquad (10)$$

where $E_i \equiv {k_i}^2$ and the limits of integration are r and R respectively.

Therefore, following equation (10), the total persistent current $I_{\rm T}$ is the current through a transverse section of the annulus.

For 2D geometries, as we have already mentioned, the effect of the number of channels on the typical currents is not yet fully understood. The number of channels M is defined as the maximum value of the transverse quantum number inside the Fermi surface at zero flux. We define the value of the Fermi energy at zero flux as $E_{\rm F} \equiv E_N$, E_N being the energy of the highest occupied level. We emphasize that in the considered isolated cavities the number of electrons N is constant for all values of the flux. For values of $\alpha \neq 0$, the average Fermi energy is defined by Weyl's formula $\langle E_{\rm F} \rangle = N/4$ (in the stipulated units) [16].

One important point is to know how M depends on the number of particles N and on the parameter λ. Employing the expansion of the zeros of the radial functions (solutions of Eq. (2)) we obtain [17]:

$$M^2 = \left[1 + \frac{4N(\lambda-1)^2}{\pi^2(\lambda^2-1)} + \left(\frac{(\lambda-1)^2}{8\pi^2\lambda} \right)^2 \right],$$

where the symbol [..] means integer part.

For $\lambda \to 1$, the second and third terms in the last equation go to 0 and we obtain the trivial result for 1D geometries, $M = 1$ independently of the number of particles N.

Most of the experimentally relevant situations involve many particles. For values of $\lambda > 1$ and for $N \gg 1$ the second term in the last expression dominates and M reads:

$$M = \left[\frac{2\sqrt{N}(\lambda-1)}{\pi\sqrt{\lambda^2-1}} \right]. \qquad (11)$$

Figure 3 shows the total current *vs.* flux for $N = 2747$ and $\lambda = 10$. This corresponds to $M = 60$. The existence of many channels implies that, opposite to what happens for 1D geometries, crossings between levels of different channels occur for $0 < \alpha < 0.5$.

Employing the expansion given by equation (4), the total current for the N electrons system can be written as:

$$I_{\rm T} = \alpha(\sum 2A_{m,n}) + \sum B_{m,n}, \qquad (12)$$

where the coefficients A's > 0, and the coefficients B's have alternated signs. The sum extends to all the filled levels N. The total current has two contributions, the first term which has an explicit linear dependence on α and the second one without explicit dependence on the flux. Nevertheless, Figure 3 shows the total current which looks like a sawtooth. Between two successive crossings the curve is a linear function with the same positive slope in each interval. The negative jumps in $I_{\rm T}$ are for values of the flux $\alpha_i^{(-)}$ where crossings between states occurs. This qualitative behaviour can be understood as follows. Let us suppose that a given state is occupied before a crossing and empty after it. This corresponds to replacing in equation (12) one value of $A_{m,n}$ by another one. As

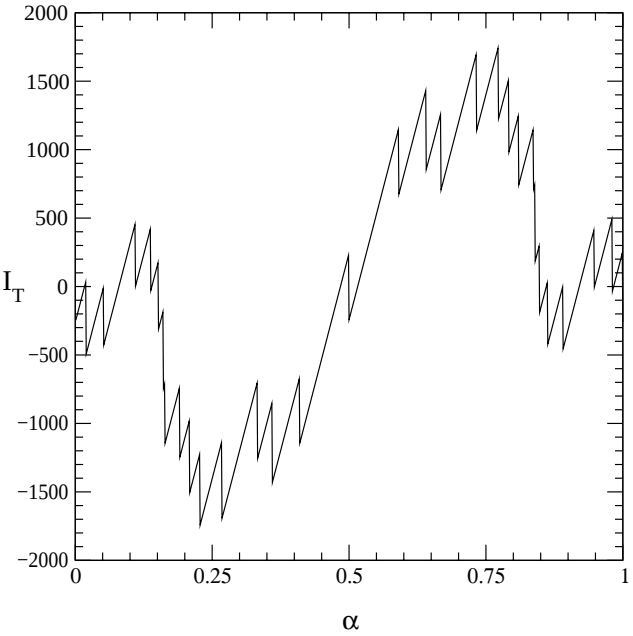

Fig. 3. Persistent current $I_{\rm T}$ as a function of the adimensional flux α for $N = 2474$ and $\lambda = 10$.

$N \gg 1$, the last replacement gives essentially the same slope. On the other hand, the second term is strongly affected because a positive value of $B_{n,m}$ is replaced by a negative one, and this produces a significative negative change in the value of the nonhomogeneous term of $I_{\rm T}$. Let us remark that between two adjacent $\alpha_i^{(-)}$'s there is another crossing at $\alpha_i^{(+)}$ that is irrelevant for $I_{\rm T}$. We denote by $n_{\rm c}^{(+)}(n_{\rm c}^{(-)})$ the total number of crossings at the positions $\alpha_i^{(+)}(\alpha_i^{(-)})$. As it will be clarified in the following sections, the features of the crossings between levels are strongly related to the shape and the magnitude of the total and typical currents.

4 The distribution of crossings

We devote this section to establish some relevant properties of the crossings between states for integrable Hamiltonian systems that depend on a single parameter. Following the semiclassical expansion for the density of states developed by Berry and Tabor for integrable systems [18], we have started writing the density of crossings per unit of energy and flux (for a given value of the parameter λ) as

$$\rho_{\rm c}(E, \alpha, \lambda) = \tilde{\rho}_{\rm c} + \rho_{\rm c}^{\rm osc};$$

$\tilde{\rho}_{\rm c}$ is the average density of crossings (where the average is taken over energy and flux) and $\rho_{\rm c}^{\rm osc}$ is the fluctuating part. We have demonstrated that

$$\tilde{\rho}_{\rm c} = C(\lambda)\sqrt{n}, \qquad (13)$$

and is independent of α [19]. Therefore the average number of crossings that a given level n has between

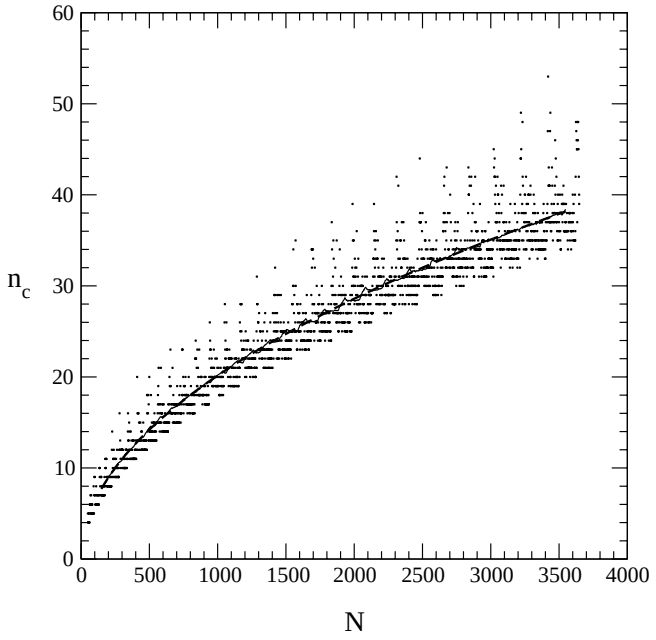

Fig. 4. Number of crossings n_c for $0 < \alpha < 1/2$ as a function of the number of levels N. The points are the exact values numerically calculated. The thin line corresponds to an average over $\Delta N = 100$ while the dashed line corresponds to the best power fit ($n_c = 0.61822 \times N^{0.50441}$) to this average. Both lines are superimposed and are almost indistinguishable.

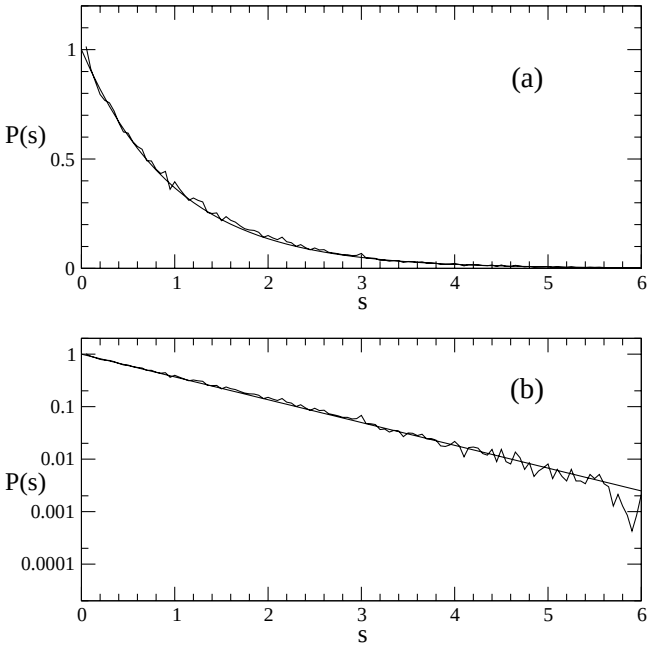

Fig. 5. (a) Nearest neighbour spacing distribution $P(s)$ numerically calculated. We also show the exact Poisson distribution $P(s) = \exp(-s)$. (b) Log-lin plot of $P(s)$.

$0 < \alpha < 0.5$ is $\tilde{n}_c = 0.5\tilde{\rho}_c$. Moreover,

$$\tilde{n}_c^{(+)} = \tilde{n}_c^{(-)} = \tilde{n}_c/2. \tag{14}$$

Figure 4 shows n_c *vs.* n, n_c being the number of crossings of the level n, for $\lambda = 10$ and $N = 3650$, together with the ensemble average $\bar{n}_c$ taken on a range $1 \ll \Delta n < N$. The best power fit to $\bar{n}_c$ is $\bar{n}_c = 0.6182 n^{\beta}$ with $\beta = 0.50441$, in strong agreement with our theoretical prediction. It is interesting to note that while the number of channels scales as $M \sim \sqrt{N}$ (see Eq. (11)), the mean number of crossings for the highest occupied level is proportional to M. This means that on average, the last occupied level experiences as many crossings as there are channels present in the system. The higher fluctuations observed in Figure 4 correspond to the apparition of a state with $m = 0$ (at $\alpha = 0$) in the energy region considered.

Another important result concerns the way in which the crossings for a given level n are distributed in the interval $0 < \alpha < 0.5$. We define the normalized nearest neighbour spacing as $s_i = \tilde{n}_c(\alpha_i - \alpha_{i-1})$, where α_i denotes the position of the crossing i. Figure 5 shows the nearest neighbour spacing distribution $P(s)$, obtained after an exhaustive numerical computation. This results in a Poisson distribution as can be checked in the mentioned figure, where the numerical result is displayed along with the exact Poisson distribution. In other words, for a given level n with n_c crossings, the corresponding α_i's can be seen as a sample of n_c uncorrelated random variables in the interval $0 < \alpha < 0.5$. Therefore, if we generalize the above definitions to n-nearest neighbour spacings as $s_i = \tilde{n}_c(\alpha_{i+n} - \alpha_i)$, the associated spacing distributions are [20],

$$P(n, s) = \frac{s^n}{n!}\exp(-s). \tag{15}$$

In the notation of the last equation $P(s) \equiv P(0, s)$. Such distributions of the spacings determine the fluctuations of the typical current, as we will show in the forthcoming section.

5 Typical currents of 2D systems and the crossings as random variables

At this point we have all the ingredients to quantify the way in which the distribution of crossings determines the scaling of the typical current with the number of particles present in the system N.

We want to compute $I^2_{\rm typ}$ (see Eq. (5)). Taking into account the definition of the total current equation (12), and the comments stated at the end of Section 3.2, we can write the square of the total current for $0 < \alpha < 0.5$ as,

$$I_T^2 = \left(A_T\alpha - F(\alpha, \alpha_i^{(-)})\right)^2, \tag{16}$$

$$F(\alpha, \alpha_i^{(-)}) \equiv \sum_{i=1}^{n_c^{(-)}} \Delta_i \Theta(\alpha - \alpha_i^{(-)}), \tag{17}$$

where we have defined $A_T \equiv 2\sum A_{m,n}$ (see Eq. (12)) and $\Theta(x)$ is the step function. The positive definite quantity

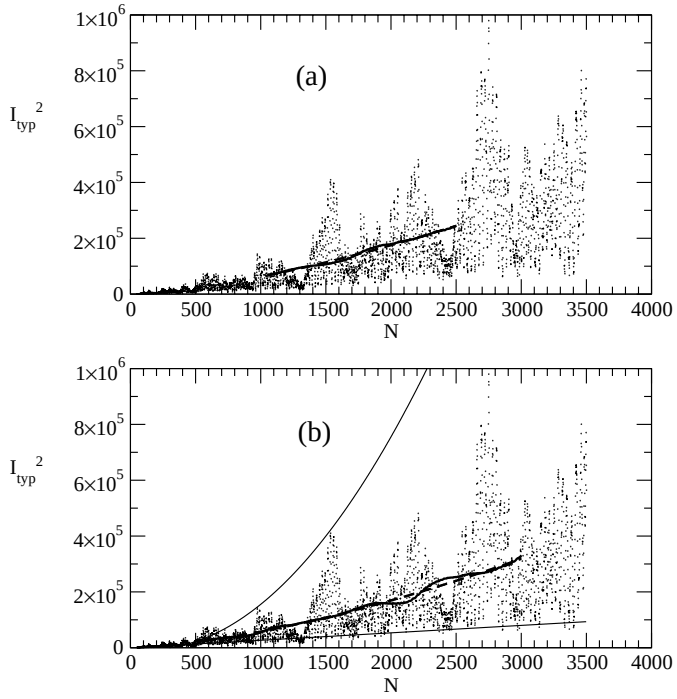

Fig. 6. (a) The square of the typical current $I^2_{\rm typ}$ as a function of N. The points correspond to exact values numerically calculated. The solid line corresponds to an N – average with $\Delta N = 2\,000$, while the dashed line is the best power fit $I^2_{\rm typ} = 2.009 \times N^{1.4966}$. Both lines are superimposed and are almost indistinguishable. (b) The same exact results of (a) but the N-average was performed with $\Delta N = 1\,000$. In this case the best power fit is $I^2_{\rm typ} = 1.7405 \times N^{1.5558}$. Here, we have drawn the limit curves ($\propto N^2$ and $\propto N$) for particular realizations of sequences α_i's.

Δ_i is the absolute value of the jump that the total current has at the position $\alpha_i^{(-)}$. As we mentioned before, all the jumps have the same negative sign, therefore we have written down a minus sign preceding the second term of equation (16). We stress that in the last equation $n_{\rm c}^{(-)}$ denotes the total number of crossings (for $0 < \alpha < 0.5$) for which $I_{\rm T}$ shows jumps. For the sake of simplicity in the notation, in the following we drop the supraindex in the $\alpha_i^{(-)}$ and in $n_{\rm c}^{(-)}$. $I_{\rm typ}$, and obviously its squared value, can be written as a function of the random variables α_i,

$$I^2_{\rm typ} = 2\left(\frac{A_{\rm T}^2}{24} + \sum_{j,i=1}^{n_{\rm c}} \Delta_i\Delta_j\left(\frac{1}{2} - {\rm Max}(\alpha_j,\alpha_j)\right) - A_{\rm T}\sum_{i=1}^{n_{\rm c}}\Delta_i\left(\frac{1}{4}-\alpha_i^2\right)\right), \quad (18)$$

where ${\rm Max}(a,b)$ means the maximum among a and b. Figure 6 shows the exact numerically obtained $I^2_{\rm typ}$ as a function of the number of particles in the system N for $\lambda = 10$. The extremely fluctuating behaviour with N is displayed.

Our aim is to determine the average dependence of $I^2_{\rm typ}$ with the total number of particles in the system N. This implies performing an average over N when the number of particles varies in a range $1 \ll \delta N < N$ (N-average). In the same figure a solid line shows this average for $\delta N \approx 2\,000$. In the present case, such a value of δN is required to obtain a smooth curve.

The fluctuations in Figure 6 are due to the different patterns of the sequences of α_i's which appear when N is varied. Therefore, we assume that the N-average is equivalent to statistical averages over different realizations of the random sequence of α_i's. We define the average typical current as

$$\hat{I}^2 \equiv \langle I^2_{\rm typ}\rangle \quad (19)$$

where the symbol $\langle..\rangle$ means average over different realizations of α_i's. $\hat{I}$ characterizes the magnitude of the current which is relevant for the experimental investigations [7].

Before computing $\hat{I}^2$, we will give a qualitative explanation of the origin of the fluctuations in $I^2_{\rm typ}$. The total current grows linearly between crossings and therefore its growth is in direct proportion to the distance between successive crossings (see Fig. 3). There are two extreme realizations of the sequence of α_i's that limit the expected behaviour of $\hat{I}^2$.

Let us first suppose that the crossings conform a regular sequence of equally spaced α_i's (what is known as a picket-fence sequence) and $\Delta_i = \Delta\ \forall i$. In this case it is easy to verify that $I^2_{\rm typ} \sim (N/n_{\rm c})^2$. As we have already stated in Section 4, $\tilde{n}_{\rm c} \sim \sqrt{N}$ (in this case $\tilde{n}_{\rm c} = n_{\rm c}$) and therefore $I^2_{\rm typ} \sim N$.

The second realization corresponds to a sequence of α_i's in which one distance between crossings is much larger than the other ones. This resembles the features of the 1D systems for which in fact, there is only one crossing in the interval $0 < \alpha < 0.5$. It is straightforward to show that for the realization considered $I^2_{\rm typ} \sim N^2$.

For the annular billiard, as we have shown in the previous section, the nearest neighbour spacing distribution between crossings is Poisson. Therefore one expects the actual behaviour of $I^2_{\rm typ}$ to be highly fluctuating with N around a mean value $\sim N^\gamma$ with $1 < \gamma < 2$. At the end of the present section we will see that equation (18), which depends on the particular realization of the sequence of α_i's, fulfills the above expectation.

In order to proceed with the computation of $\hat{I}^2$, it is necessary to assume some behaviour for the amplitudes Δ_i. In Figure 3, it can be seen that the amplitudes of the jumps are not essentially very different on average. This fact suggests us to assume

$$\Delta_i = \Delta = \frac{A_{\rm T}}{2\tilde{n}_{\rm c}}, \quad (20)$$

$\forall i$. This ansatz will be strongly justified by our results.

From equation (18) and performing the ensemble average over α_i's we obtain:

$$\hat{I}^2 = 2\left(\frac{A_{\rm T}^2}{24} - \frac{A_{\rm T}}{4}\Delta\tilde{n}_{\rm c} + A_{\rm T}\Delta\left(\sum_{j=1}^{\tilde{n}_{\rm c}}\langle\alpha_{2j-1}^2\rangle\right) + \frac{\Delta^2}{2}\tilde{n}_{\rm c}^2 - \Delta^2\left(\sum_{j=1}^{\tilde{n}_{\rm c}}(2j-1)\langle\alpha_{2j-1}\rangle\right)\right), \quad (21)$$

where the sums run over the odd values because we have assumed that the odd crossings contribute to the jumps in the total current (it is worth noting that the election is arbitrary and an equivalent treatment assuming jumps in the even crossings gives the same results).

To evaluate $\langle\alpha_{2j-1}\rangle$ and $\langle\alpha_{2j-1}^2\rangle$ we have considered $\alpha_{2j-1} = s_{2j-1}$, where s_{2j-1} is the spacing between the crossing in $\alpha = 0$ and the crossing in $\alpha = \alpha_{2j-1}$. Therefore, employing the distributions equation (15) (adequately normalized to nearest neighbour mean spacing $d = 1/(4\tilde{n}_{\rm c})$) we have obtained:

$$\sum_{j=1}^{\tilde{n}_{\rm c}}(2j-1)\langle\alpha_{2j-1}\rangle = d\left(\frac{4}{3}\tilde{n}_{\rm c}^3 - \frac{1}{3}\tilde{n}_{\rm c}\right)$$
$$\sum_{j=1}^{\tilde{n}_{\rm c}}\langle\alpha_{2j-1}^2\rangle = d^2\left(\frac{4}{3}\tilde{n}_{\rm c}^3 + \tilde{n}_{\rm c}^2 - \frac{1}{3}\tilde{n}_{\rm c}\right), \quad (22)$$

here we have employed

$$\langle\alpha_{2j-1}\rangle = d(2j-1),$$
$$\langle\alpha_{2j-1}^2\rangle = d^2 2j(2j-1). \quad (23)$$

After replacing equation (22) in equation (21) we finally obtain:

$$\hat{I}^2 = 2\left(\frac{A_{\rm T}^2}{24} + \frac{\Delta^2\tilde{n}_{\rm c}^2}{6} - \frac{A_{\rm T}\Delta\tilde{n}_{\rm c}}{6} + \frac{A_{\rm T}\Delta}{16} + \frac{\Delta^2}{12} - \frac{A_{\rm T}\Delta}{48\tilde{n}_{\rm c}}\right). \quad (24)$$

The above expression allows us to classify each term according to the dependence on N. Taking into account equations (13, 14, 20) and the fact that $A_{\rm T} \propto N$, we can verify that each of the first three terms in the equation (24) are of order $\mathcal{O}(N^2)$ and that their total contribution vanishes. The fourth term is of order $\mathcal{O}(N^{3/2})$ and the two last ones are $\mathcal{O}(N)$. We have obtained for the mean typical current,

$$\hat{I}^2 = \frac{A_{\rm T}^2}{16\tilde{n}_{\rm c}} + \frac{A_{\rm T}^2}{48\tilde{n}_{\rm c}^2}, \quad (25)$$

and therefore for large N,

$$\hat{I}^2 \sim \mathcal{O}(N^{3/2}).$$

Equation (25) constitutes one of the main results of the present article. We have plotted in Figure 6a, besides the exact numerical results (dots), the N-average with $\delta N = 2\,000$ (solid line) together with its best power fit $\sim N^\gamma$ (dashed line). The resulting value for the exponent is $\gamma = 1.498$ in strong agreement with our theoretical result.

At this point, let us mention that the choice of $\delta N = 2\,000$ to perform the N-average could seem somehow ambiguous. However, if we perform an N-average with $\delta N < 2\,000$, although the resulting curve displays oscillations, the best fit leads to the same scaling with N (see Fig. 6b). It is important to remark that equation (18) can be employed to evaluate the typical persistent current for a given realization of the α_i's. In particular for the picket-fence sequence (note the absence of the ensemble average in the following),

$$\sum_{j=1}^{\tilde{n}_{\rm c}}(2j-1)\alpha_{2j-1} = d\left(\frac{4}{3}\tilde{n}_{\rm c}^3 - \frac{1}{3}\tilde{n}_{\rm c}\right)$$
$$\sum_{j=1}^{\tilde{n}_{\rm c}}\alpha_{2j-1}^2 = d^2\left(\frac{4}{3}\tilde{n}_{\rm c}^3 - \frac{1}{3}\tilde{n}_{\rm c}\right). \quad (26)$$

The last equations lead to a cancellation of all the orders greater than $\mathcal{O}(\mathcal{N})$ in equation (18) for $I_{\rm typ}^2$. That is

$$I_{\rm typ}^2 = \frac{A_{\rm T}^2}{48\tilde{n}_{\rm c}^2}\,. \quad (27)$$

Equation (27) satisfies $I_{\rm typ}^2 \sim N$ in accordance with our previous qualitative discussion (see the paragraph below Eq. (19)).

On the other hand, we expect some other particular realizations of the sequence of α_i's for which there is no cancellation of the terms of order $\mathcal{O}(N^2)$ in equation (18). In this case $I_{\rm typ}^2 \sim N^2$.

We stress that the considered particular realizations manifest themselves when $I_{\rm typ}^2$ takes the lowest and highest values respectively (see Fig. 6b).

6 Concluding remarks

In the present work we have characterized the behaviour of the persistent current for a system of non-interacting electrons confined in a mesoscopic bi-dimensional clean cavity as a function of the number of particles in the system N. We have deduced relevant properties of the single particle spectrum such as the scaling of the number of open channels M and average number of level crossings $\tilde{n}_{\rm c}$ with N.

The main goal of this article has been to determine the N-average behaviour of the typical current through the statistical properties of the degeneracies present in the single particle spectrum as a function of the flux, when many channels are relevant. We can separate the dependence on N of the typical current in two contributions. The first one is the average value taking on a range $1 \ll \delta N < N$ and constitutes the smooth contribution. The second one, depends on the particular realization of the sequence of crossings α_i's (the values of flux where degeneracies in

the spectrum occur) and leads to an extremely fluctuating behaviour with N. We have related this fact to the statistics of the distribution of crossings which, as we have determined is Poissonian. The smooth part of the typical current has been obtained under the assumption that the ensemble average over different realizations of the random sequence of crossings α_i's is equivalent to the N-average. The obtained dependence on N of this smooth contribution is $\hat{I}^2 \sim N^{3/2}$ which is in strong agreement with the numerical results (see Fig. 6). On the other hand we have evaluated the typical current for particular realizations of sequences of α_i's which lead to completely different dependence on N, namely $I^2_{\rm typ} \sim N^2$ and $I^2_{\rm typ} \sim N$. These realizations are responsible for the large oscillations of $I^2_{\rm typ}$.

Last but not least, some words of caution are in order in connection with experimental observations of persistent currents. It is necessary to emphasize that, owing to the extreme sensitivity of the typical current on the particular realization of α_i's, any experiment devoted to establish the scaling of the average typical current on N (or on the number of open channels M) in mesoscopic 2D cavities would involve measurements on the order of thousands of samples (remember that $\delta N \approx 2\,000$, for the annular geometry).

This work was partially supported by UBACYT (TW35), PICT97 03-00050-01015 and CONICET. We would to thank G. Chiappe for useful discussions.

References

1. M. Büttiker, Y. Imry, M.Ya. Azbel, Phys. Rev. A **30**, 1982 (1984).
2. S. Washburn, R.A. Webb, Phys. Today **41**, 46 (1988).
3. N. Byers, C.N. Yang, Phys. Rev. Lett. **7**, 46 (1961).
4. M. Büttiker, Y. Imry, R. Landauer, Phys. Rev. A **96**, 365 (1983).
5. L.P. Levy, G. Dolan, J. Dunsmuir, H. Bouchiat, Phys. Rev. Lett. **64**, 2074 (1990).
6. V. Chandrasekar *et al.*, Phys. Rev. Lett. **67**, 3578 (1991).
7. D. Mailly, C. Chapelier, A. Benoit, Phys. Rev. Lett. **70**, 2020 (1993).
8. K. Richter, D. Ullmo, R.A. Jalabert, Phys. Rep. **276**, (1996).
9. T. Guhr, A. Müller-Groeling, H.A. Weidenmüller, Phys. Rep. **299**, 189 (1998).
10. H.F. Cheung, Y. Gefen, E.K. Reidel, Wei-Heng Shih, Phys. Rev. B **37**, 6050 (1988).
11. H.F. Cheung, Y. Gefen, E.K. Reidel, IBM J. Res. Develop. **32**, 359 (1988).
12. H. Bouchiat, G. Montambaux, J. Phys. France **50**, 2695 (1989).
13. E. Louis, J.A. Vergés, G. Chiappe, Phys. Rev. B **11**, 6912 (1998).
14. A.J.S. Traiber, A.J. Fendrik, M. Bernath, J. Phys. A **22**, L365 (1989).
15. E. Merzbacher, *Quantum Mechanics* (Wiley, New York, 1970).
16. H.P. Baltes, E.R. Hilf, *Spectra of finite systems* (Bibliographisches Institut, Mannheim, 1976).
17. M. Abramowitz, I.A. Stegun, *Handbook of Mathematical functions* (Dover, New York, 1972).
18. M.V. Berry, M. Tabor, Proc. Roy. Soc. London A **349**, 101 (1976).
19. A.J. Fendrik, M.J. Sánchez, preprint `quant-ph/9908044`.
20. M.L. Mehta, *Random Matrices* (Academic Press, Inc., 1991).